Supporting Information for

Assembly of Micro-Carbonized Lignin-Cellulose Mixture and Carbon Nanotubes via Interfacial Interactions to Prepare Composite Film with Superior Electromagnetic Interference Shielding and Mechanical Performance

Tianyu Zhang[a,b], Xu Zhang[a,b], Huanxin Huo[a,b], Guanben Du[a,b], Jianyong Wan[a,b], Long Yang[a,b,*]

[a] Yunnan Province Key Lab of Wood Adhesives and Glued Products, International Joint Research Center for Biomass Materials, School of Materials and Chemical Engineering, Southwest Forestry University, Kunming 650224, China

[b] Key Laboratory for Forest Resources Conservation and Utilization in the Southwest Mountains, Ministry of Education, Southwest Forestry University, Kunming 650224, China

* Corresponding authors

E-mail: lyang@swfu.edu.cn (L. Yang)

Table of contents

Methods

Materials

Sodium carboxymethyl cellulose (CMC) was purchased from Macklin (Shanghai, China). Sodium lignosulfonate was purchased from Sigma-Aldrich (Shanghai, China). Carbon nanotubes (CNT, purity: > 97%, diameter: 1-2 nm) was purchased from Chengdu Organic Chemicals Co., Ltd (Chengdu, China). All other solvents (DMF, DCM, THF and CH_3OH, etc.) were supplied by Tianli Chemical Reagent Co., Ltd. (Tianjin, China). Deionized water, prepared using a Master Q30UT water purification system (Hitech Instruments Co., Ltd., Shanghai, China), was used for all experiments.

Preparation of LCD nanoparticles

A solution of Sodium lignosulfonate (0.3 g) in H_2O (50 mL) was reacted at 180 °C for 8 h in a high-pressure reactor. After cooling naturally to room temperature, carbon dots (LCD) was obtained by evaporating the solvent.

Preparation of LCCD chains

A solution of Sodium lignosulfonate (0.1 g) and CMC (0.2 g) in H_2O (50 mL) was reacted at 180 °C for 8 h in a high-pressure reactor. After cooling naturally to room temperature, a novel carbon dots (LCCD) was obtained by evaporating the solvent.

Fabrication of CMC-CNT film

The mixture of CMC (10 mg mL^{-1}, 7 mL) and CNT (5 mg mL^{-1}, 6 mL) was ultrasonicated for 30 minutes to ensure complete dissolution. As-obtained mixture was vacuum filtered to obtain CMC-CNT film. Finally, the deposited film was immersed in acetone bath for several times to dissolve the cellulose membrane, and

then the CMC-CNT film was then annealed at 80 ℃ for 6 h.

Fabrication of CMC-L-CNT film

The mixture of CMC (10 mg mL^{-1}, 7 mL), Sodium lignosulfonate (L, 10 mg) and CNT (5 mg mL^{-1}, 6 mL) was ultrasonicated for 30 minutes to ensure complete dissolution. As-obtained mixture was vacuum filtered to obtain CMC-L-CNT film, Finally, the deposited film was immersed in acetone bath for several times to dissolve the cellulose membrane, and then the CMC-L-CNT film was then annealed at 80 ℃ for 6 h.

Fabrication of CMC-LCD-CNT film

The mixture of CMC (10 mg mL^{-1}, 7 mL), LCD (10 mg) and CNT (5 mg mL^{-1}, 6 mL) was ultrasonicated for 30 minutes to ensure complete dissolution. As-obtained mixture was vacuum filtered to obtain CMC-LCD-CNT film. Finally, the deposited film was immersed in acetone bath for several times to dissolve the cellulose membrane, and then the CMC-LCD-CNT film was then annealed at 80 ℃ for 6 h.

Fabrication of CMC-LCCD-CNT film

The mixture of CMC (10 mg mL^{-1}, 7 mL), LCCD (10 mg) and CNT (5 mg mL^{-1}, 6 mL) was ultrasonicated for 30 minutes to ensure complete dissolution. As-obtained mixture was vacuum filtered to obtain CMC-LCCD-CNT film, Finally, the deposited film was immersed in acetone bath for several times to dissolve the cellulose membrane, and then the CMC-LCCD-CNT film was then annealed at 80 ℃ for 6 h. Here, the CMC-LCCD-CNT film with different CNT content (10 wt%, 20 wt%, 30 wt%

and 40 wt%) were fabricated using similar methods, respectively.

Characterization

Scanning electron microscopy (SEM) images were obtained using a GeminiSEM 300 field emission scanning electron microscope (ZEISS Co., Ltd., Germany). Transmission electron microscopy (TEM images) were obtained using a JEM-2100 transmission electron microscope (JEOL Ltd., Tokyo, Japan), at an accelerating voltage of 200 kV. XRD patterns were recorded on an X-ray diffractometer (Rigaku D/max 2550 V, Cu Kα radiation, λ = 1.54178 Å). The XRD analysis was performed with scanning speed of 5°/s, scanning step size of 0.02° and 2θ range of 5-85°. XPS measurements were performed using an X-ray photoelectron spectrometer (ESCALAB 250Xi, Thermo Scientific). Fourier-transform infrared (FT-IR) spectra were collected using a Nicolet iS10 FT-IR spectrometer. Samples were scanned over the range of 550-4000 cm^{-1}, with a resolution of 4 cm^{-1}. Uniaxial tensile measurements were carried out using Electronic Universal Testing Machine (Suns Technology Stock Co., Ltd. Shenzhen, China), with an extension rate of 100 mm/min. The EMI shielding performance of the composites from 8.2 to 12.4 GHz (X band) were characterized by using a network vector analyzer (Agilent Technologies N5244A) based on ASTM D4935-10 standard, through recording its scattering parameters (S_{11} and S_{21}). The wide-angle X-ray scattering (WAXS) data of films were collected on the WAXS beamline at the Australian Synchrotron (Melbourne, Australia), using 18.1 keV beam energy (wavelength 0.685 Å) and a Dectris-Pilatus3

X 2M (253.7 × 288.8 mm; 1475 × 1679 pixels) detector. The data was integrated along the meridional and equatorial directions in the ±5° region using X-ray Microdiffraction Analysis Software (XMAS) to identify the anisotropic scattering.

Calculation of electromagnetic interference shielding effectiveness (EMI SE)

The proposed EMI shielding mechanism of composite was shown in Supplementary Fig.18, on the basis of its brick-and-mortar microstructure characteristics. A part of the electromagnetic waves was reflected back due to impedance mismatch while the incident electromagnetic waves were exposed to composite. The residual electromagnetic (EM) waves passed though and interact with CNT networks, leading to conductance and polarization loss. Meanwhile, the transmission path of electromagnetic waves increased after multiple internal reflections and scattering due to the brick-and-mortar microstructure of composite and the interface between the conductive CNT and the insulating polysaccharide chain, which then reinforced the absorbing attenuation of EM waves.

EMI shielding performance of materials strongly depends on its electrical conductivity. The EMI shielding was mainly determined by reflection SE (SE_R) and absorption SE (SE_A) combined with the reflection coefficient (R), absorption coefficient (A), and transmission coefficient (T) for composites. Such a prominent EMI SE can be explained via the Simon formula:

$$SE = 50 + 10\,lg(\sigma/f) + 1.7t\,(\sigma \times f)^{1/2} \quad (1)$$

where σ is the electrical conductivity in S cm^{-1}; f is the frequency of electromagnetic waves in GHz; and t is the thickness of EMI shielding materials in cm. From the Simon formula, t and σ of the shielding materials are the determinants of EMI SE at a given frequency.

The network analyzer method is a common technique used for the far-field EMI SE measurement. The EMI SE in the far field can be calculated by the measured *S*-parameters (S_{11}, S_{21}, S_{22}, S_{12}) from a vector network analyzer, where, S_{ij} indicates the transmission from port *j* to port *i*. Here, j designated the network analyzer port receiving the EMI radiation, and j represents the port that was transmitting the incident energy. Based on the *S*-parameters, the reflectance (R), absorbance (A) and transmittance (T) can be calculated:

$$R = |S_{11}|^2 = |S_{22}|^2 \tag{2}$$

$$T = |S_{12}|^2 = |S_{21}|^2 \tag{3}$$

$$A = 1 - R - T \tag{4}$$

The reflection loss (SE_R), the absorption loss (SE_A), multiple internal reflection loss (SE_M) and the total shielding effectiveness (SE) could be calculated:

$$SE_R = -10\lg(1-R) = -10\lg\left(1-|S_{11}|^2\right) \tag{5}$$

$$SE_A = 10\lg\left(\frac{1-R}{T}\right) = 10\lg\left(\frac{1-|S_{11}|^2}{|S_{12}|^2}\right) \tag{6}$$

$$SE = SE_A + SE_R + SE_M \tag{7}$$

While $SE_A > 10$ dB, SE_M could be neglected.

The specific shielding effectiveness (SSE) was calculated by dividing SE with the composite density (d). To account for the thickness contribution (t), the following equation was used to evaluate the absolute effectiveness (SSE t^{-1}) of composites:

$$SSE|t = \frac{SE}{dt} \tag{8}$$

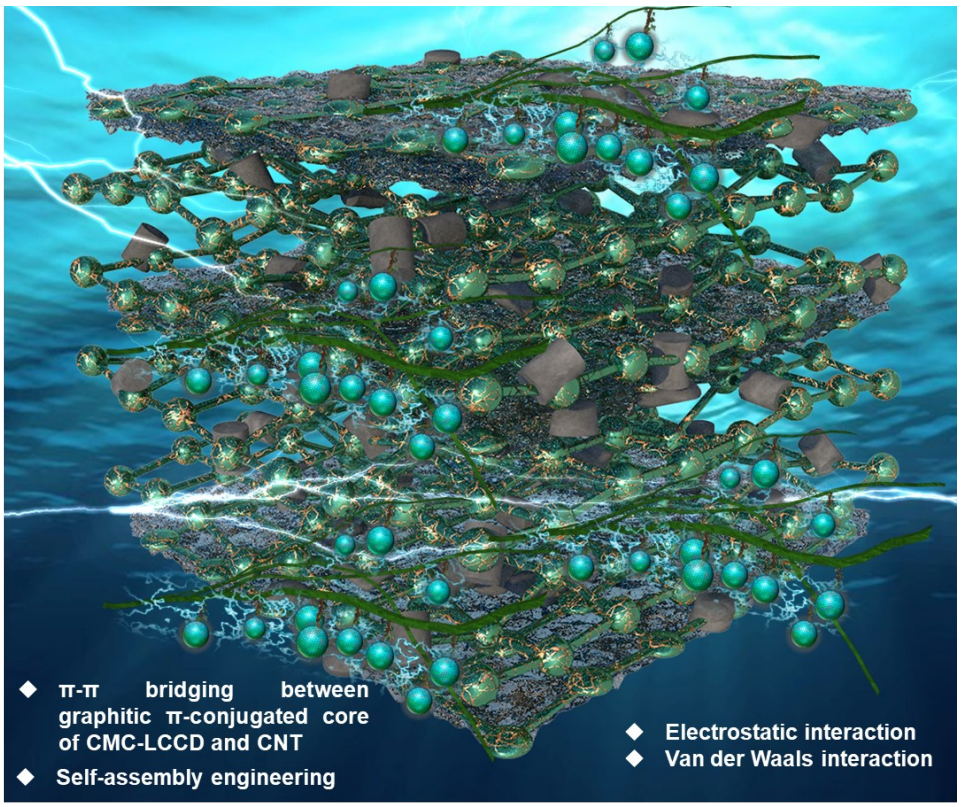

Figure. S1. Engineering EMI shielding and mechanical performance of CMC-LCCD-CNT film by interfacial interactions.

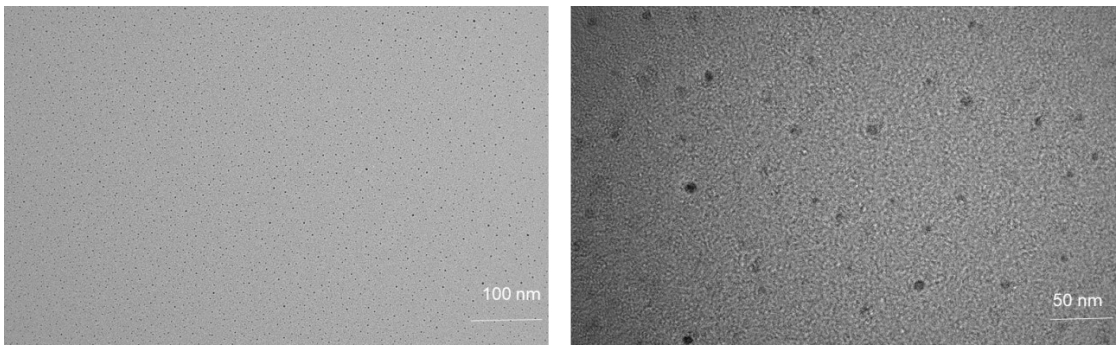

Figure. S2. TEM of LCCD chains.

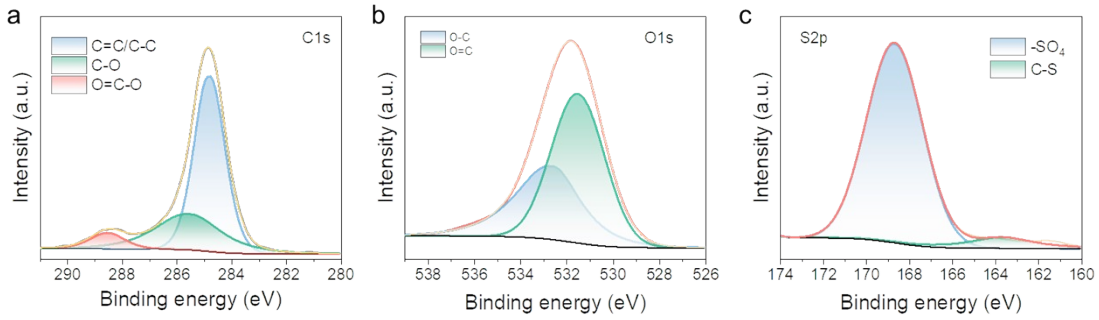

Figure. S3. XPS of LCCD chains including high resolution on C1s scan (a), O1s scan (b) and S2p scan (c).

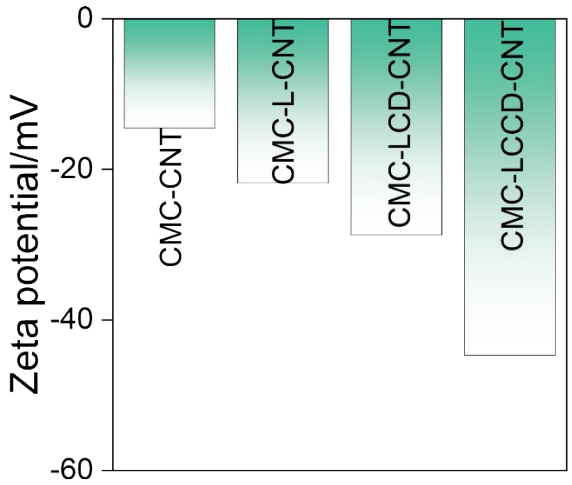

Figure. S4. Zeta potential of CMC, LCCD, and CNT, indicating good electrostatic compatibility.

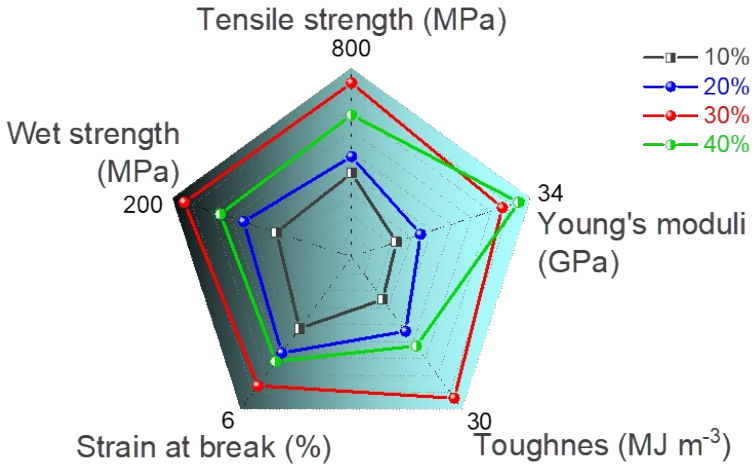

Figure. S5. Radar image of comparison of tensile strength, Youg's moduli, toughness, strain at break, and wet strength performance of CMC-LCCD-CNT film for different CNT concentration.

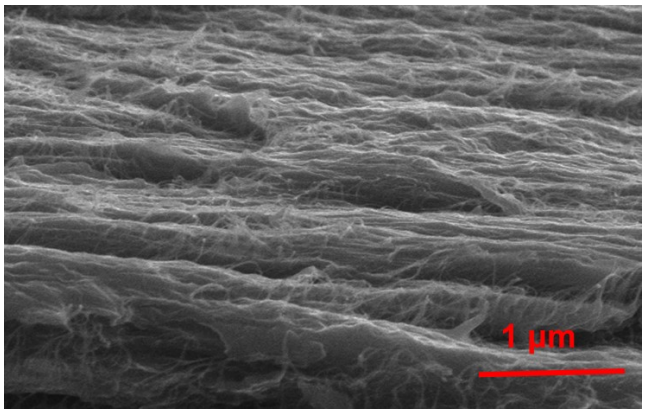

Figure. S6. SEM pattern of CMC-LCCD-CNT film, scale bar = 1 µm.

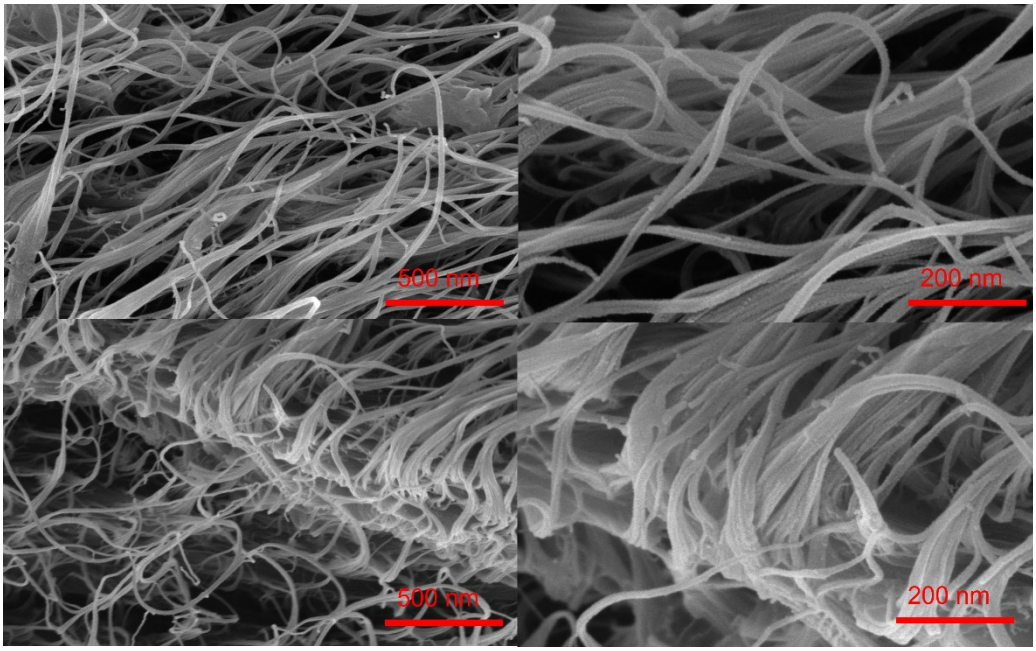

Figure S7. Cross-sectional SEM images of CMC-LCCD-CNT film at 500 nm and 200 nm scales, showing a well-ordered lamellar "brick-and-mortar" structure with CNTs embedded in the polymer matrix.

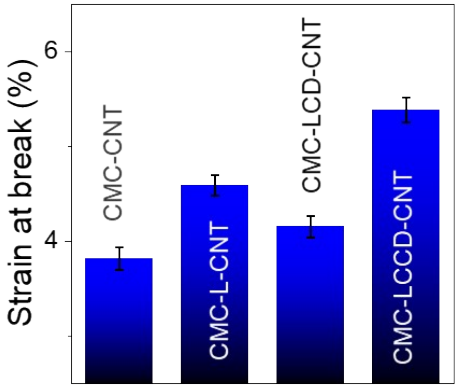

Figure. S8. Tensile strain of CMC-CNT, CMC-L-CNT, CMC-LCD-CNT, and CMC-LCCD-CNT films.

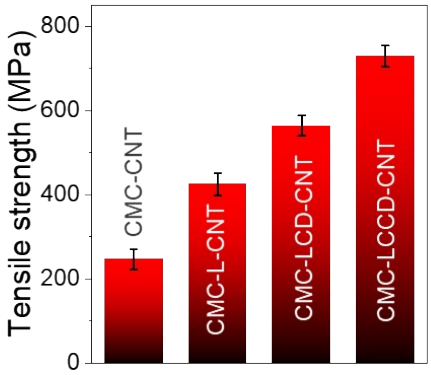

Figure. S9. Tensile strength of CMC-CNT, CMC-L-CNT, CMC-LCD-CNT, and CMC-LCCD-CNT films.

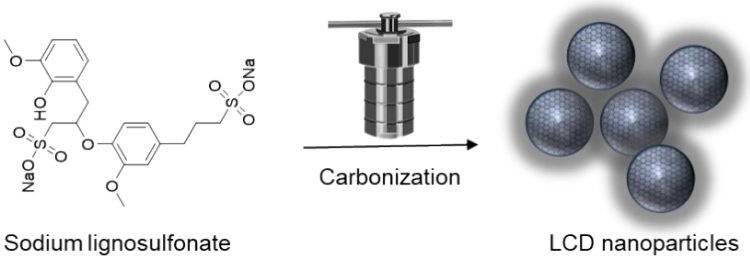

Figure. S10. The preparation of LCD nanoparticles using sodium lignosulfonate as feedstock.

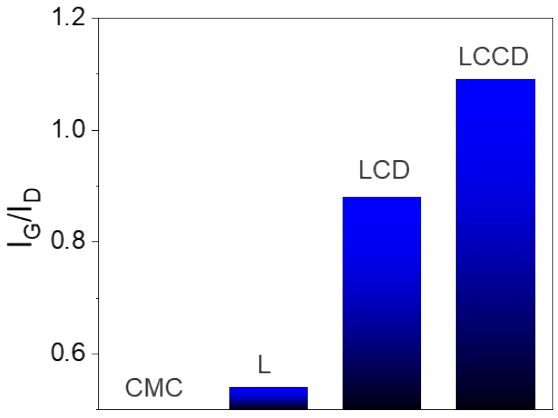

Figure. S11. The ratio of G and D characteristic peak from Raman spectra for CMC, sodium lignosulfonate (L), LCD and LCCD.

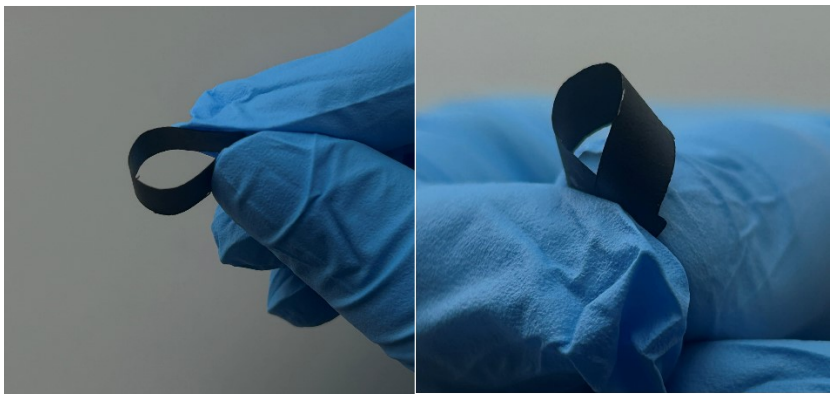

Figure S12. Bending test of CMC-LCCD-CNT film, showing high flexibility without fracture.

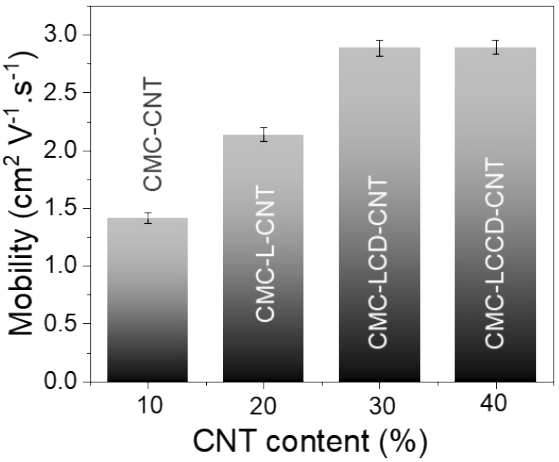

Figure. S13. Comparison of mobility of CMC-LCCD-CNT film for different CNT concentration.

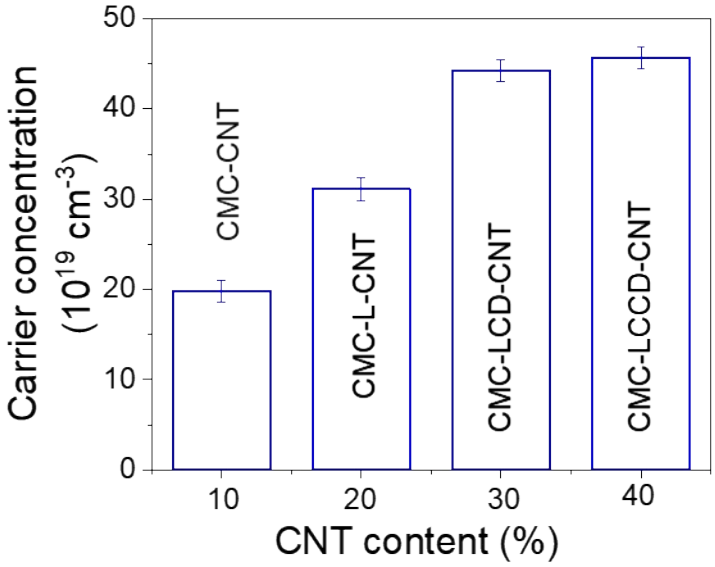

Figure. S14. Comparison of carrier concentration of CMC-LCCD-CNT film for different CNT concentration.

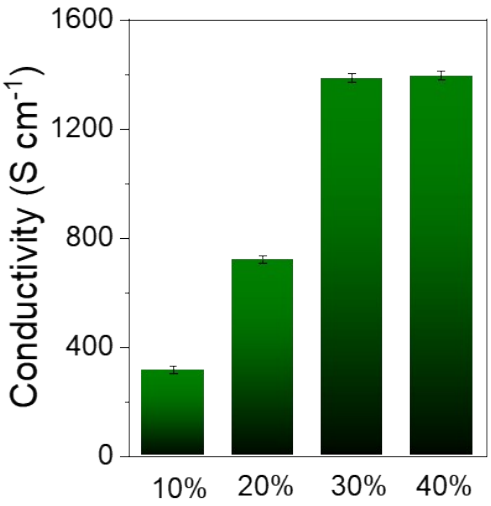

Figure. S15. Comparison of conductivity of CMC-LCCD-CNT film for different CNT concentration.

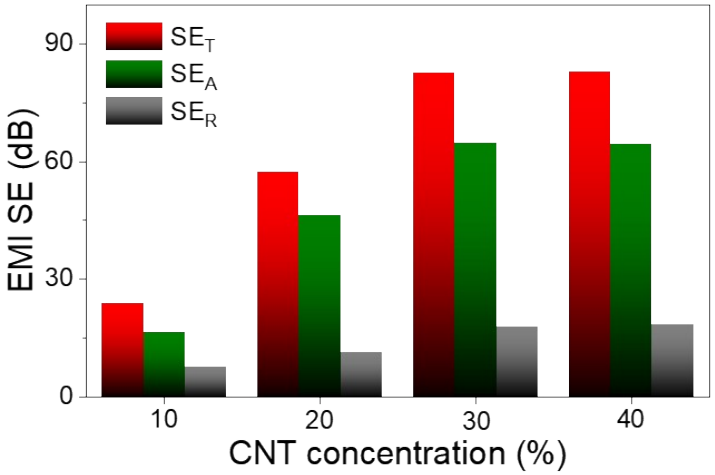

Figure. S16. SE_T, SE_R, and SE_A values of CMC-LCCD-CNT with different CNT content.

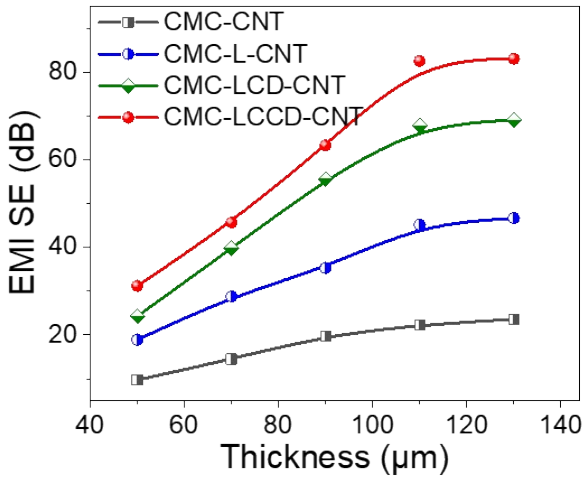

Figure. S17. EMI shielding performance of CMC-CNT, CMC-L-CNT, CMC-LCD-CNT and CMC-LCCD-CNT films with different thickness.

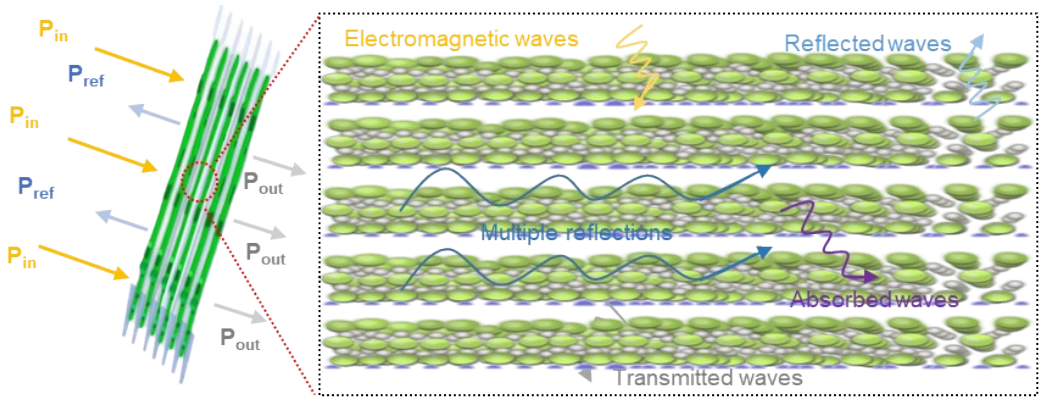

Figure. S18. Schematic illustration of the electromagnetic wave transfer across the composites "brick-and-mortar" structure.

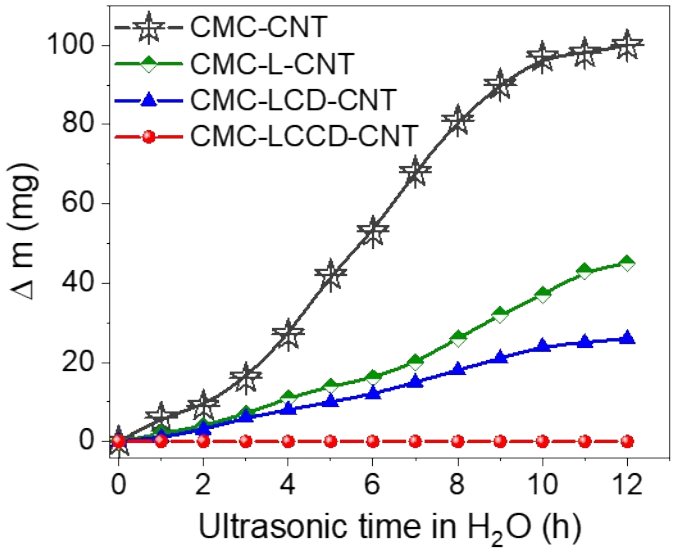

Figure. S19. Mass changes of CMC-CNT, CMC-L-CNT, CMC-LCD-CNT and CMC-LCCD-CNT films ultrasonicated for different time in H_2O.

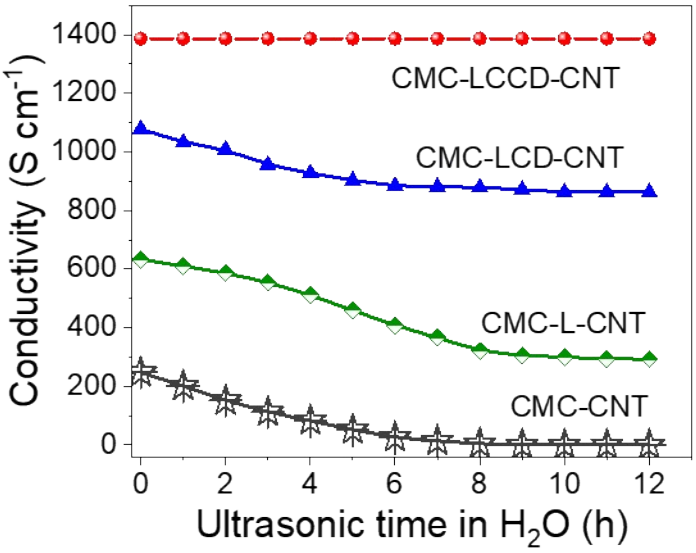

Figure. S20. Conductivity of CMC-CNT, CMC-L-CNT, CMC-LCD-CNT and CMC-LCCD-CNT films ultrasonicated for different time in H_2O.

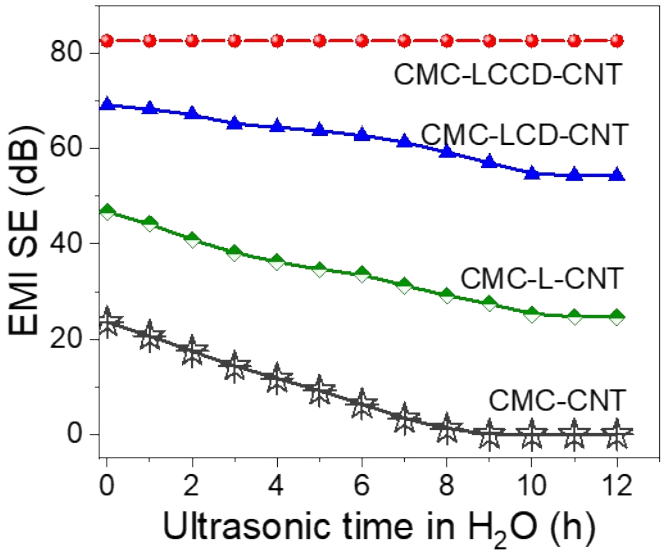

Figure. S21. EMI shielding performance of CMC-CNT, CMC-L-CNT, CMC-LCD-CNT and CMC-LCCD-CNT films ultrasonicated for different time in H_2O.

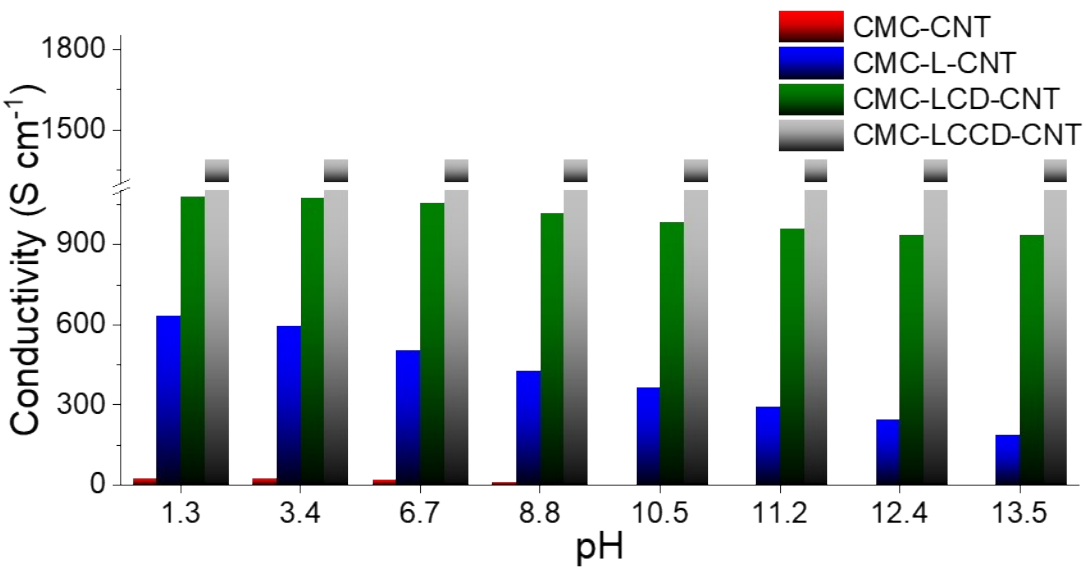

Figure. S22. Conductivity of CMC-CNT, CMC-L-CNT, CMC-LCD-CNT and CMC-LCCD-CNT films immersed in acid or alkali solution.

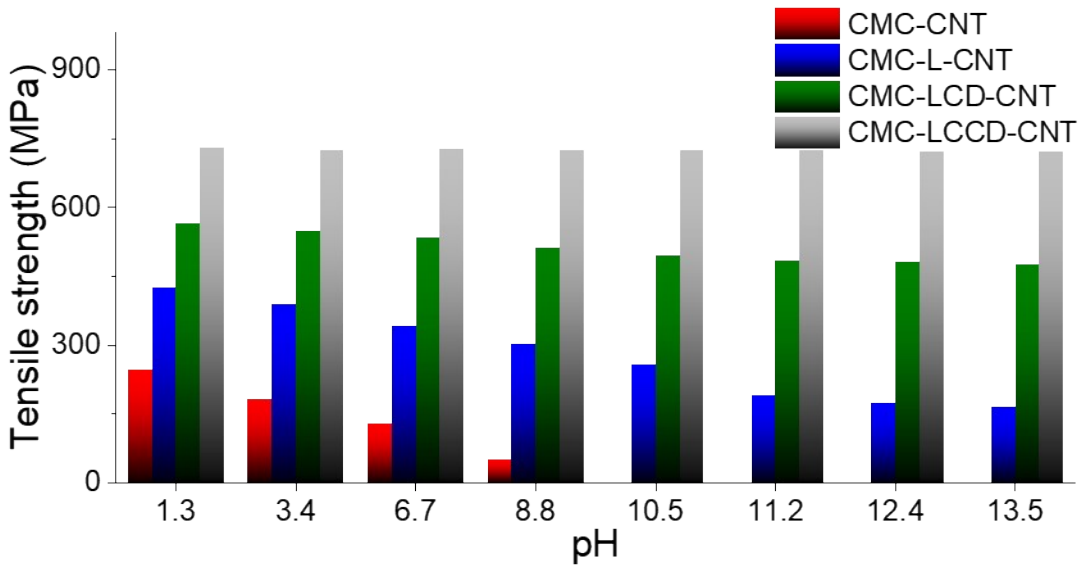

Figure. S23. Tensile strength of CMC-CNT, CMC-L-CNT, CMC-LCD-CNT and CMC-LCCD-CNT films immersed in acid or alkali solution.

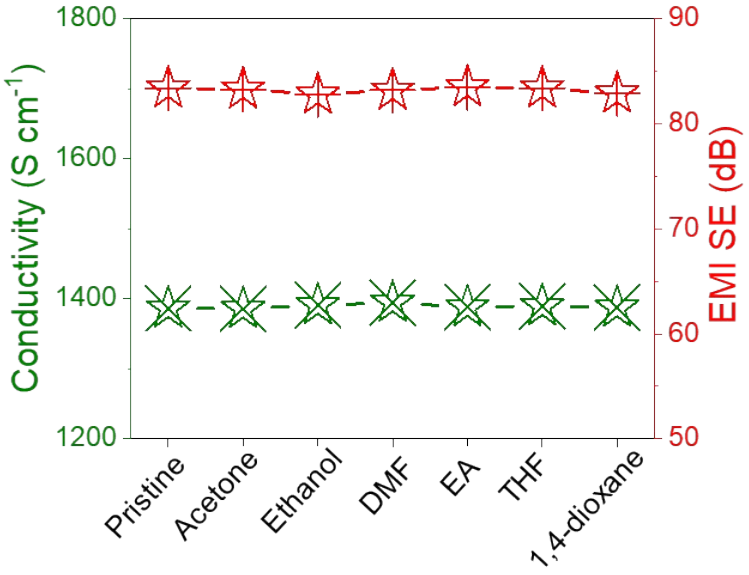

Figure. S24. Conductivity and EMI SE performance of CMC-LCCD-CNT film after immersing in different organic solution for 12 h.

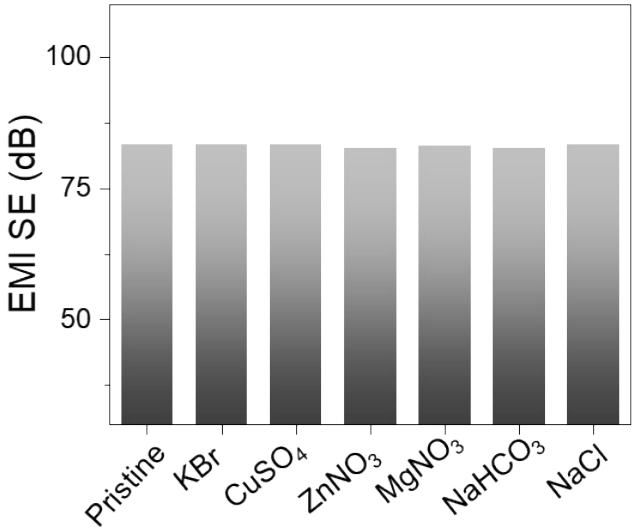

Figure. S25. Conductivity and EMI SE performance of CMC-LCCD-CNT film after immersing in different salty solution solution for 12 h.

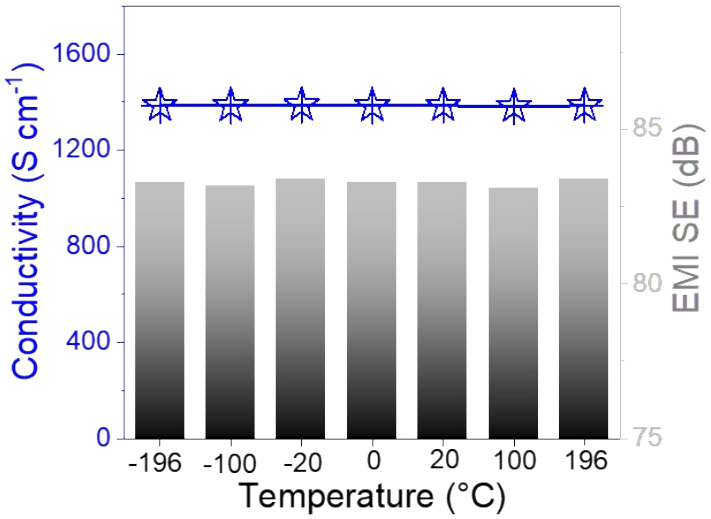

Figure. S26. Conductivity and EMI SE performance of CMC-LCCD-CNT film treated at different temperature for 12 h.

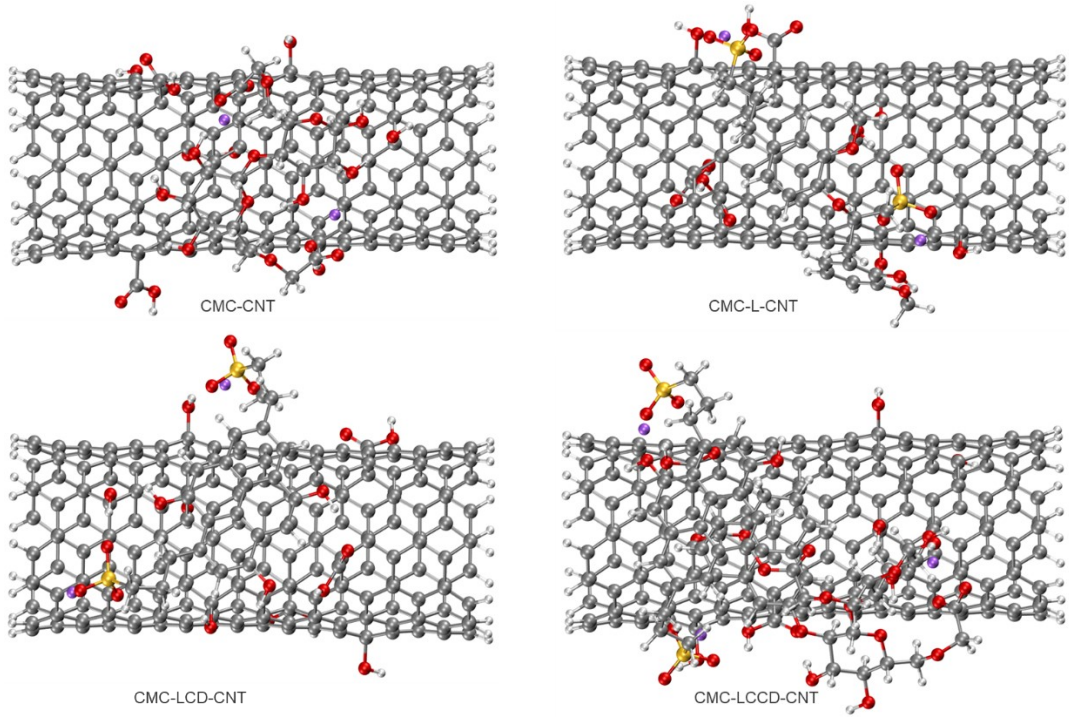

Figure. S27. The interaction performance between CNT and optimized model molecules of CMC- CNT, CMC-L-CNT, CMC-LCD-CNT and CMC-LCCD-CNT films using for ab-initio molecular dynamic simulations and independent gradient model (IGM).

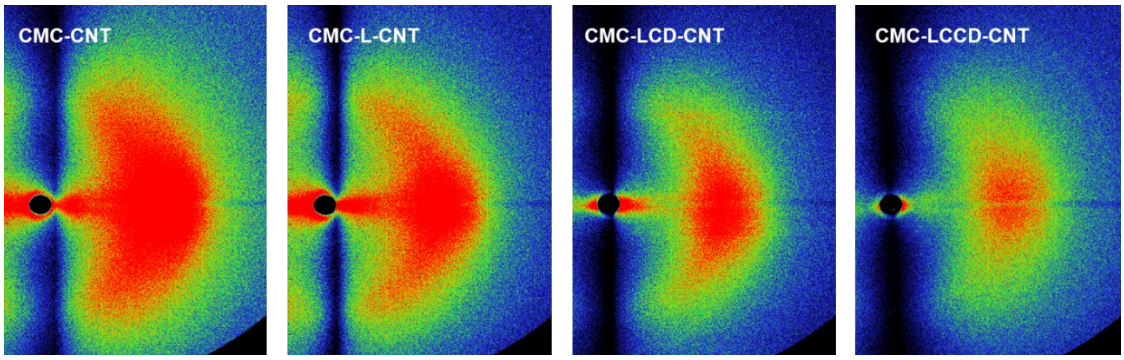

Figure. S28. Azimuthal scan wide-angle X-ray scattering (2D-WAXS) patterns (for a rotating anode X-ray source) showing the full width at half maximum (FWHM) of CMC-CNT, CMC-L-CNT, CMC-LCD-CNT and CMC-LCCD-CNT films.